

Towards the interrogation of the behaviour of a single nanoparticle under realistic catalytic reaction conditions

David James Martin, Donato Decarolis, Remi Tucoulou, Gema Martínez-Criado & Andrew M. Beale

To cite this article: David James Martin, Donato Decarolis, Remi Tucoulou, Gema Martínez-Criado & Andrew M. Beale (2017) Towards the interrogation of the behaviour of a single nanoparticle under realistic catalytic reaction conditions, *Catalysis, Structure & Reactivity*, 3:1-2, 63-70, DOI: [10.1080/2055074X.2016.1277655](https://doi.org/10.1080/2055074X.2016.1277655)

To link to this article: <https://doi.org/10.1080/2055074X.2016.1277655>



© 2017 The Author(s). Published by Informa UK Limited, trading as Taylor & Francis Group



[View supplementary material](#)



Published online: 21 Feb 2017.



[Submit your article to this journal](#)



Article views: 394





[View Crossmark data](#)



Citing articles: 2 [View citing articles](#)

Towards the interrogation of the behaviour of a single nanoparticle under realistic catalytic reaction conditions

David James Martin^{a,b†} , Donato Decarolis^{a,b†}, Remi Tucoulou^c, Gema Martínez-Criado^{c,d} and Andrew M. Beale^{a,b} 

^aDepartment of Chemistry, University College London, London, UK; ^bResearch Complex at Harwell (RCaH), Didcot, UK; ^cEuropean Synchrotron Radiation Facility, Grenoble, France; ^dInstituto de Ciencia de Materiales de Madrid, Consejo Superior de Investigaciones Científicas, Cantoblanco, Spain

ABSTRACT

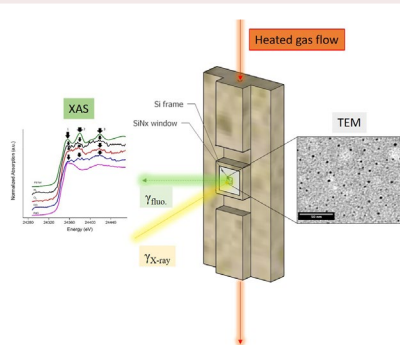
It is well known that particle size plays an important role in catalytic activity although the reason(s) why significant changes in activity are observed to occur with small changes in size are not well understood. The presence of particular facets, metal-support interactions, and redox state etc., are also capable of playing a role. The difficulty in realising which features are pertinent in a catalytic process stems from issues regarding sample complexity in typical heterogeneous catalysts, as well as technical challenges with instruments used to investigate samples in terms of their sensitivity and capability to distinguish between a specific vs. ensemble response in catalytically active vs. spectator species. We show here how the combination of using a synthesis method which achieves a discrete dispersion of metal Pd nanoparticles with a very narrow particle size distribution ($\sigma \sim 1$ nm) in combination with nano-beam X-ray spectroscopy allows us to follow the changes in redox state with time. Importantly, the data are obtained in one example, from an illuminating spot containing ca. 20 nanoparticles with an extremely small size distribution.

ARTICLE HISTORY

Received 17 October 2016
Accepted 20 December 2016

KEYWORDS

Pd nanoparticles; nano-XANES; particle size; *in situ*



1. Introduction


Precious metal nanoparticles comprising Pt, Au, Pd etc. supported on light metal oxides (i.e. Al_2O_3 , SiO_2 , TiO_2) form the basis of many types of critical industrial heterogeneous catalyst systems. In order to gain a working insight into the nature of the active component in the system, research efforts have been directed towards studying catalysts using nanoparticle sensitive X-ray synchrotron based techniques such as XAS (X-ray Absorption Spectroscopy) amongst others [1]. Numerous examples exist in the literature which

testify that the size and/or shape of the nanoparticle is an important parameter influencing catalytic activity [2–6]. It is also well known that nanoparticles actively respond to their environment *in situ*, often changing shape so as to maximize, for example, the contact area of a particular surface, e.g. the (111) surface [7]. In the majority of these studies however, the preparation methods used to make these catalysts result in nanoparticles with large particle size distributions (standard deviation, $\sigma > 1$ nm), essentially masking the importance of a particular particle size or shape on activity. Typically,

CONTACT Andrew M. Beale  Andrew.Beale@ucl.ac.uk

[†] Current address: Van 't Hoff Institute for Molecular Sciences, University of Amsterdam, Amsterdam, Netherlands.

Processed XANES/EXAFS data can be found from the following link. [<http://tiny.cc/YCSR-1277655>]

 Supplemental data for this article can be accessed at <http://dx.doi.org/10.1080/2055074X.2016.1277655>

© 2017 The Author(s). Published by Informa UK Limited, trading as Taylor & Francis Group.

This is an Open Access article distributed under the terms of the Creative Commons Attribution License (<http://creativecommons.org/licenses/by/4.0/>), which permits unrestricted use, distribution, and reproduction in any medium, provided the original work is properly cited.

arithmetic mean particle sizes of a set of nanoparticle catalyst samples are identified via electron microscopy, together with ranges and/or standard deviations, and then it is often attested that the difference in catalytic activity is likely due to the variation in mean particle sizes between samples. However, a paradox intrinsically arises as within the range, there exists many sub-species of particle sizes, which in some cases could in fact be more catalytically active than the “identified” mean particle size. For example recently, Rogers et al. used a common colloidal method to prepare realistic catalyst nanoparticles, with a small standard deviation in particle size ($\sigma \sim 0.6$ nm), but a relatively large range. Such a synthesis technique is commonly used, however, the authors utilized HR-HAADF-STEM (High Resolution-High Angle Annular Dark Field-Scanning Transmission Electron Microscopy) to highlight the existence of a very active sub-species of atomic Au clusters (1–5 atoms), which can in some samples increase the turnover frequency 10-fold [8]. Cutting edge synthesis techniques such as reverse micelle metal ion encapsulation, first demonstrated by Spatz et al., generate nanoparticle populations with suitably small particle size distributions ($\sigma \ll 1$ nm), and critically, completely encapsulate all metal ions which prevents the development of sub-species by virtue of an water-in-oil system where solubility is fully controlled [9].

State of the art nano-beamlines such as the insertion device line ID16B-NA (ESRF) now possess the ability to perform conventional X-ray based techniques, such as XAS and XRD (X-ray diffraction), with extremely fine spatial resolution – with beam sizes in the range of 10s of nanometers [10,11]. The relevance to catalysis is that conventional X-ray “bulk” techniques, with large beams (mm- μ m), are prone to statistical averaging effects where important insight into the behaviour of nanoparticles under process conditions can be lost against a background of sample components that either do not respond to their catalytic environment or else respond differently, i.e. are spectator species which play little role in the catalytic process under investigation. Whilst techniques such as Transmission Electron Microscopy (TEM) might conceivably be considered to be capable of providing some of this information, it is often difficult to obtain such data under the relevant process conditions (although we acknowledge that with the development of environmental TEM this is becoming steadily more obtainable) and that it does not provide the sought-after chemical information on the active state of the catalyst [12]. Advances in other techniques such as Scanning Transmission X-ray Microscopy (TXM) or X-ray computed tomography have been steadily increasing the available spatial resolution for studying small catalysts bodies on the μ m scale with a view to eventually studying isolated working nanoparticulate catalysts in order to elucidate the true active regions and eliminate statistical

averaging effects (see reviews and references therein [13–15]). Hence, there is a real and well documented driving force for the use of nano-beam spectroscopic techniques for interrogating catalyst samples.

Even if it were possible to interrogate a single particle there is the question as to whether it is catalytically interesting/representative or not. A compromise in this quandary can be best realised via a combination of using an advanced synthetic method that generates a population of nanoparticles (with small standard deviation) and a nano-beam X-ray facility primarily to tackle the question of the importance of a particular particle size on catalytic activity. Here we report our attempts of characterising, using nano-beam XAS (ca. 400×400 nm², fluorescence mode), a sample of size-controlled palladium nanoparticles patterned onto an atomically flat, X-ray transparent SiN_x window, and mounted on a custom-built gas-flow reactor cell also under separate reducing and oxidizing atmospheres. We therefore demonstrate a study where particle size distribution effects are all but eliminated; showing it is possible and indeed beneficial to study a small population (ca. ~20 nanoparticles) of nanoparticle catalysts, as uncommon spectral features are identified.

2. Methodology

2.1. Sample preparation

A modified reverse-micelle method, originally developed by Spatz et al., was used to synthesise Pd nanoparticle-micelle-toluene mixtures [16,17]. To prepare a typical reverse micelle solution, a 0.5 polymer wt. % solution (5 mg/mL) of diblock copolymers (Polymer Source Inc.) was prepared by dissolving poly-styrene-*b*-poly(2-vinylpyridine; “PS-*b*-P2VP”), of different molecular weight and polymer chain lengths (e.g. 30-*b*-8.5 g/mol or 175-*b*-75 g/mol), where the chain length is multiplied by 1000) in toluene for 24 h. Afterwards, a specific ratio of metal atoms (K₂PdCl₆, Sigma-Aldrich 99%) per pyridine unit, metal loading ratio, (e.g. 0.3:1 or 0.1:1) was added to the solution and stirred for another 48 h, allowing for the incorporation of [PdCl₆]²⁻ into the reverse micelle cores, forming a complex with pyridine. After complexation of Pd into the core, a reductant (P-Toluene Sulfonyl Hydrazide, Sigma-Aldrich, 97%) was added in a 4:1 ratio (to Pd), and then finally 100 μ L of HCl (Sigma-Aldrich, ACS reagent grade, 37%) was added in order to stabilize the micelles. This solution was then stirred for 1 h, leading to the formation of one nanoparticle per reverse micelle. Two stock solutions were prepared using the aforementioned method and are henceforth labelled as “SS-A” and “SS-B”. SS-A was prepared using a polymer solution of 30–8.5 (PS-*b*-P2VP), and a metal loading of 0.3:1. SS-B was synthesised using a larger diblock copolymer, 175-*b*-75 (PS-*b*-P2VP), and had a metal loading of 0.1:1. According to the synthesis method, SS-A will yield smaller and more densely packed nanoparticle arrays

than SS-B, which will have comparatively larger particles which are more dispersed. Therefore, any potential particle size effects of gas adsorption, or inter-particle effects could potentially be studied under operating conditions.

Two samples (“A-1” and “B-2”) to be tested using nanobeam XAS were then prepared as follows; Pd nanoparticle populations were coated onto 0.5×0.5 mm SiN_x windows supported on 1 cm^2 silicon wafers (Norcada Inc.), using a “drop-cast” method with the two different stock solutions SS-A and SS-B [9]. Sample A-1 was prepared using SS-A, and then air-plasma treated (100 W, 10 min, 300 mTorr) in order to remove the micelles on the surface. Sample B-1 was made using SS-B, and also left untreated with micelles intact. Samples A-1 and B-1 were then characterised on ID16B-NA (ESRF).

In addition, to verify the reliability and reproducibility of the spectra obtained, Pd nanoparticles supported on powdered Si_3N_4 was prepared (denoted herein as sample “A-2”), and subsequently characterised on B18 at DLS (Diamond Light Source. This sample was prepared mixing the stock solution SS-A with powdered Si_3N_4 (Silicon (IV) nitride, amorphous, 98.5 + %, 15–30 nm APS powder, S.A. 103–123 m^2/g , Alfa Aesar) in order to obtain a 1% metal/support weight ratio. The sample was then left to stir-dry overnight and subsequently calcined for 2.5 h at 500 °C in a muffle furnace.

2.2. Sample characterisation

Ex situ TEM measurements were conducted on a JEOL-2100 at 200 kV, using 300 square mesh carbon-copper grids. A drop of the Pd-micelle solution (either SS-A, or SS-B) was dropped onto the grid and analysed after

evaporation. In both instances, copper grids were used in TEM analysis, as Si-SiN_x windows (7.5×7.5 mm) are too large to fit in conventional TEM holders. Mean particle diameter (d_p), standard deviation (σ), and average radial distance of 1st nearest neighbour (r_{mn}) were calculated using ImageJ.

In situ XAS was performed on sample A-2 on B18 at DLS in transmission mode. The supported palladium nanoparticle catalyst was sieved using a fraction of 125/250 μm , and then loaded into a quartz capillary and mounted on a catalysis testing station, with the capillary inlet connected to gas lines on one side and a residual gas analyser (Mass Spectrometer) on the outlet. While under helium flow, the palladium catalysts were brought to an operating temperature of 343 K. Subsequently, different gas compositions (5% H_2 in helium, 10% oxygen in helium, and 5% CO in helium) were passed through the catalyst and XAFS spectra were recorded at steady state for each gas composition. Data were then analysed using the Demeter package; Athena for XANES normalization and linear combination was fitting and Artemis for EXAFS fitting [18]. Linear combination fitting involves fitting the unknown/intermediate spectra as an algebraic combination of known spectra, such as standard references.

2.3. Nanofocus beamline cell design and data acquisition protocol

A vertical gas-flow cell was designed for *in situ*/operando XAFS (in either fluorescence or transmission mode) measurements of Pd nanoparticles deposited on SiN_x windows (Figure 1(a)). The cell was purposely small

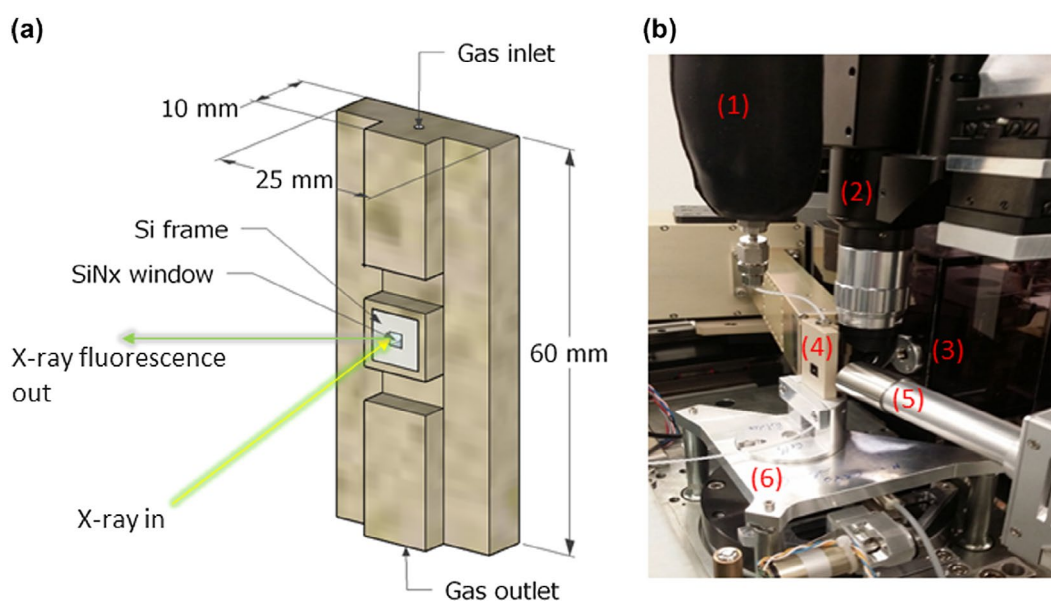


Figure 1. (a) Schematic of the gas flow cell used on ID16B-NA. Gas flows from top to bottom, across the SiN_x window which is loaded with Pd particles. (b) Close up of the reactor set up. The gas flows in from the heated tubing at the top, passes across the Pd- SiN_x window and out through the bottom to exhaust. Two XRF detectors (single and multi-element array) are positioned extremely close to the front-side window at ca. 15° to collect as high quality data as possible.

Key: (1) heated inlet, (2) optical microscope for selection of the region of interest, (3) KB mirror box, (4) reactor cell, (5) single element detector, (6) x, y, z-stage.

(60 × 25 × 10 mm) so as to be compatible with the components of a nanofocus spectroscopy beamline, such as XRF detectors, focusing Kirkpatrick-Baez mirrors and support stages (Figure 1(b)). In order to avoid strong X-ray absorption and/or secondary fluorescence, the cell was fabricated from PEEK (polyether ether ketone), which is also lightweight and chemically inert. SiN_x X-ray transparent windows (in a silicon wafer frame) were used as a substrate for mounting the Pd nanoparticles as they are chemically inert, low stress (< 250 MPa), and most importantly the window depth can be made extremely thin (10–50 nm) to acquire X-ray fluorescence signal without compromising durability and/or strength (e.g. attenuation length at 24.3 keV is 2 mm). The Si-SiN_x frames were then fixed using epoxy resin onto the PEEK flow reactor and attached to a moveable nano-positioning stage. Mass flow controllers (“MFCs”; Brooks GF40) were used to control gas flow and composition, and connected to the cell using 1/16” PTFE tubing and Swagelok connecting unions. The gas was brought up to operating temperature (343 K) using an insulated heating hose (1 m, 1/4” diameter, K-type thermocouple, closed pore silicone foam rubber heat insulation; PE Heated Hoses Ltd). An exit line was connected to an exhaust to ensure removal of gaseous waste and/or products. Flow rates were set at a maximum of 7 ml/min using the MFCs (GHSV ca. 100 h⁻¹).

XANES spectra were acquired on ID16B-NA (ESRF) in fluorescence mode for samples A-1 and B-1. The X-ray beam size used was 400 × 400 nm² and Pd locations were found by scanning horizontally/vertically and tracking the X-ray fluorescence detector count rate for Pd (Hitachi Vortex 90-EX). Initially, the beam was focused at 50 × 70 nm, however, fluorescence yield was low at this spot size as not enough palladium nanoparticles were illuminated. A typical scan at the Pd-K edge (24.35 keV) would scan from 24.3 to 24.46 keV (the energy range is

deliberately small to prevent beam drift). First, the catalyst was treated with zero grade helium at 360 K to clean the Pd catalysts (7 ml/min). After which, XANES scans were recorded for each gas mixture (4% H₂ in helium, 10% O₂ in helium and 10% CO in helium), each scan taking ~9 min. to complete (10 s/point, 338 points) and repeated six times in order to obtain a final summed spectrum.

3. Results

First we discuss the characterisation of the stock solutions in terms of the size of the Pd nanoparticles that the synthesis approach yields, before discussing how this particle size is maintained when the particles are subsequently transferred to high surface area Si₃N₄ powders or SiN_x reactor windows.

3.1. TEM analysis of Pd nanoparticles obtained from stock solutions SS-A & SS-B

Figure 2 (a) and (b) contain TEM images of the two Pd nanoparticle-containing stock solutions used in this study (SS-A and SS-B) after deposition on a carbon-copper TEM grid. Whilst SS-A contains Pd nanoparticles with a mean particle size (d_p) of 2.3 ± 0.6 nm and a mean separation (r_{nm}) of 18.6 ± 5.1 nm, SS-B contains larger particles (d_p of 5.6 ± 1.1 nm) which are more dispersed (r_{nm} of 92.1 ± 18.1 nm). We note that in SS-B some of the particles appear to have undergone double nucleation containing two particles in very close proximity to each other. Since these distances are too small to resolve accurately, their distance of separation is not included in the calculation of r_{nm} in this sample. Figure ESI 1 also contains a TEM image of the A-2 sample, which with a d_p value of 2.8 ± 0.8 nm, suggests that the method to produce the Pd nanoparticles is robust enough to withstand

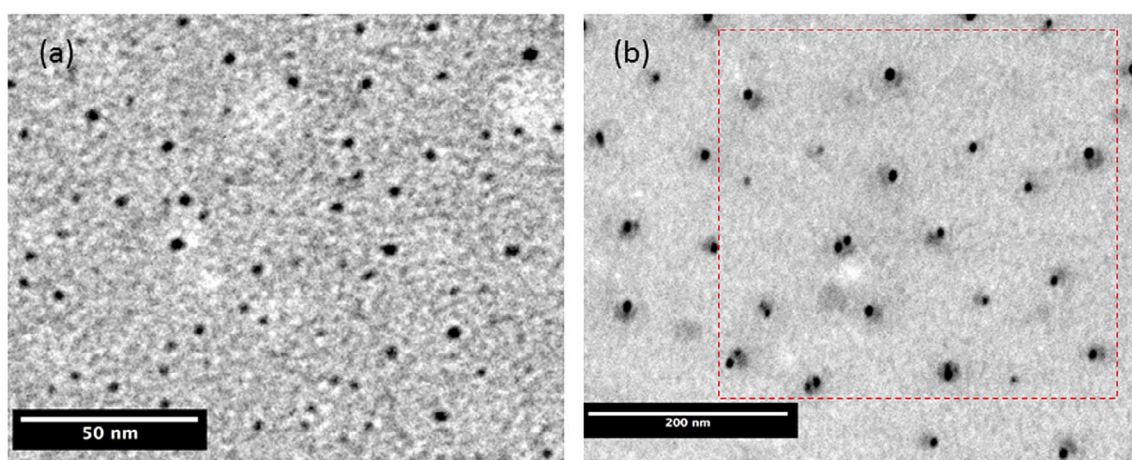


Figure 2. TEM images of Pd nanoparticles on carbon-copper TEM grids; (a) SS-A ($d_p = 2.3 \pm 0.6$ nm, $r_{nm} = 18.6 \pm 5.1$ nm). (b) SS-B ($d_p = 5.6 \pm 1.1$ nm, $r_{nm} = 92.1 \pm 18.1$ nm).

For reference, the approximate beam footprint (400 × 400 nm) used on ID16B-NA is illustrated in (b) as a red dashed line.

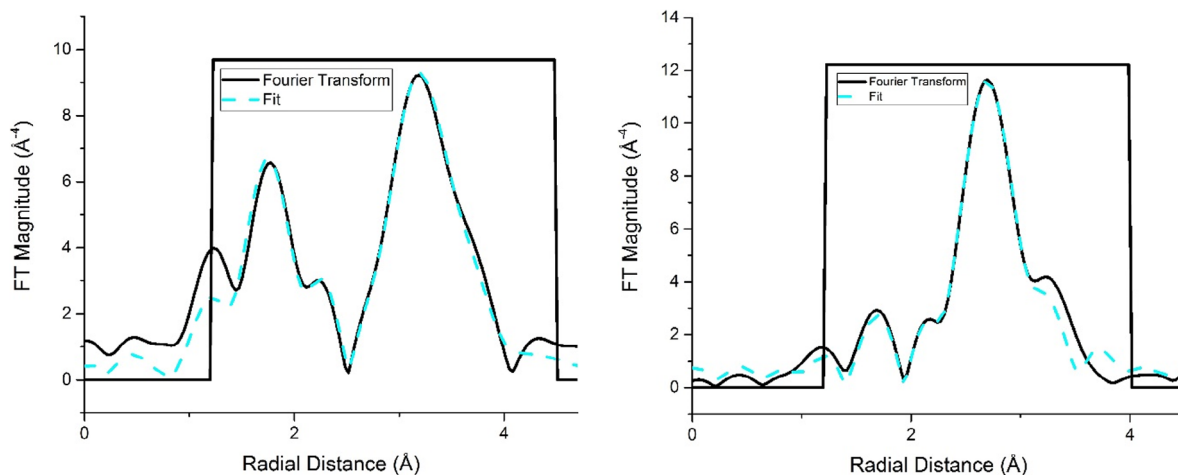


Figure 3. Left, R-space fit of sample A-2 under He flow and right, under H₂. Note, the peak at ~3.0 Å (not phase corrected) in the FT on the left is confirmation for the presence of PdO in the sample.

Table 1. EXAFS fit obtained from sample A-2 under different gas atmospheres. After H₂ flow, the sample is reduced from PdO to Pd metal, evidenced by the loss of a CN_{Pd-O} contribution as well as the appearance of two R_{Pd-Pd} scattering paths typical of Pd metal XAFS.

Refined parameter											
Gas	CN _{Pd-O}	R _{Pd-O} (Å)	σ ² (Å ²)	CN _{Pd-Pd}	R _{Pd-Pd} (Å)	σ ² (Å ²)	CN _{Pd-Pd}	R _{Pd-Pd} (Å)	σ ² (Å ²)	R-factor	
He	3.7 ± 0.7	2.027 ± 0.017	0.0027 ± 0.002	2.3 ± 1.9	3.095 ± 0.004	0.007 ± 0.004	4.1 ± 1.4	3.49 ± 0.02	0.003 ± 0.002	0.054	
Particle size estimation (nm)											
	CN _{Pd-Pd}	R (Å)	σ ² (Å ²)	Particle size estimation (nm)		R-factor					
H ₂	9.6 ± 1.9	2.75 ± 0.009	0.00802 ± 0.001	2.4 ± 0.5		0.06					

the transfer to a powdered catalyst support, however, due to the irregular surface of the support it is not possible to obtain a meaningful value for r_{nm} .

3.2. XAFS analysis of Pd nanoparticles supported on silicon nitride powder

Figure 3 contains the fitted EXAFS FT (Fourier Transform) data for sample A-2 under a He and H₂ atmosphere taken at B18, Diamond Light Source. Under He, the sample is essentially PdO, as evidenced by the high intensity of the Pd–O scattering peak, located at ~2.01 Å. Under H₂, the contribution at 2.01 Å drops in intensity and concomitantly a peak due to Pd–Pd scattering at 2.75 Å emerges, demonstrating that the Pd environment in sample A-2 is predominantly metallic [19]. Figure ESI 3 also shows the XANES linear combination fits of A-2 under hydrogen and helium atmospheres, with each respective atmosphere corresponding to fully reduced Pd metal, and a fully oxidised Pd (PdO). Table 1 and Figure 3 shows the results from a least squares fitting of the EXAFS data for sample A-2 under He and H₂, where the first shell coordination number (N) is subsequently extracted. The average particle size was estimated via the coordination number, assuming the particle to be isotropic, using the method by Beale and Weckhuysen [20]. The obtained value, 2.4 ± 0.5 nm, is remarkably consistent with the results obtained from the flat substrate TEM data shown in Figure 2(a),

demonstrating excellent agreement between the number-averaged TEM data and the bulk-averaged XAFS data and therefore is testimony of the robustness of the preparation method irrespective of the physical nature of the substrate.

3.3. Nanobeam XANES measurements of samples under reactive gas atmospheres

XAFS data were collected on samples A-1 and B-1 (Si₃N₄ window located on the reactor cell window) at 293 K under He flow, and under different atmospheres at 343 K (H₂, O₂, CO and a reactive mixture of CO and O₂) using a 400 × 400 nm² square beam. From the TEM image (Figure 2(b)) the number of nanoparticles in the field of view for the two samples are ca. 200 particles for SS-A, and ca. 20 for SS-B respectively.

Figure 4 shows XANES spectra of sample A-1 and A-2 as well as XANES spectra from Pd foil and PdO standard. The data obtained for sample A-1 is noisy as the spectra is only collected from ca. 150 particles, however, it is clear that there are several characteristic “peaks” (continuum resonances and scattering features) primarily located at 24.36, 24.38 and 24.42 keV respectively, ascribable to metallic Pd. On switching gas to O₂, whilst the XANES features at 24.38 and 24.42 keV remain essentially unchanged, there is a small increase in the feature (the rising absorption edge) at 24.36 keV which can be understood in terms of the formation of

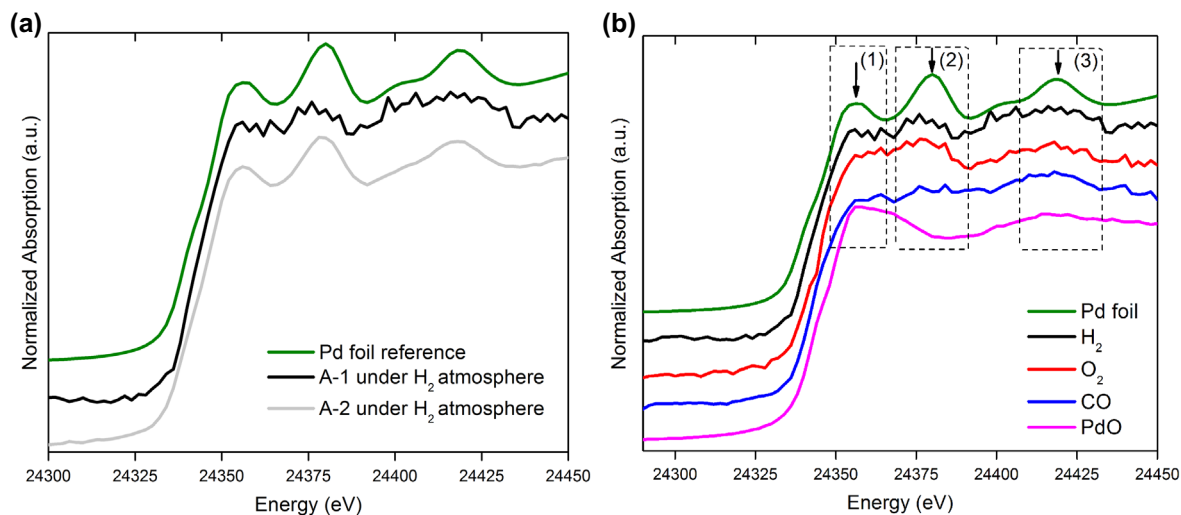


Figure 4. (a) Normalized XANES spectra of sample A-1 and A-2 against a palladium foil reference. (b) XANES spectra of sample A-1 under different atmospheres, including Pd foil and PdO standard; arrows point out the Pd XANES features at: (1) 24.36 keV; (2) 24.38 keV; (3) 24.42 keV. All spectra are vertically offset by an arbitrary value for clarity.

Table 2. Linear combination fit applied to the XANES data for sample A-1, recorded under various atmospheres and using bulk PdO and metallic Pd foil as references.

Sample atmosphere	Weight Pd metal (%)	Weight PdO (%)	R-Factor
H ₂	72.9 ± 8.3	27.01 ± 8.3	0.0108
O ₂	33.4 ± 9.6	66.6 ± 9.6	0.0057
CO	72.3 ± 9.9	27.7 ± 9.9	0.0081

more PdO species; note that a lack of change in the intensity of the 24.38 and 24.42 features which are caused by Pd–Pd scattering, points towards the formation of PdO species at the nanoparticle surface. A further gas switch to CO sees a reduction in the intensity of all three features (in relation to the sample in both H₂ and O₂ atmospheres) which can be best understood in terms of a reduction/removal of surface oxide species and the formation of Pd metal/PdC species. A more quantitative analysis to determine the degree of oxidation/reduction, using linear combination fitting with two standards (Pd metal and PdO) was then performed. The results from this fitting are given in Table 2 and shown in Figure ESI 2. The analysis shows that around the composition of the system under H₂ comprises that of ~73% of Pd metal and ~27% of PdO, whilst in an O₂ atmosphere the composition varies to of approximately 66% PdO and 44% Pd metal. After flowing CO over the nanoparticulate catalysts, the ratio of metal to oxide returns to 66 and 30% respectively as a result of re-reduction of the surface. It is also noted that the XANES spectrum of sample A-1 shows a potential shift towards higher energies when the nanoparticles are exposed to CO, as shown in the close-up (Figure 5). According to Bugaev et al. this ca. 1 eV shift in the first near edge peak could be explained by a formation of PdC carbide, as a consequence of the adsorption of CO on the Pd nanoparticles [21].

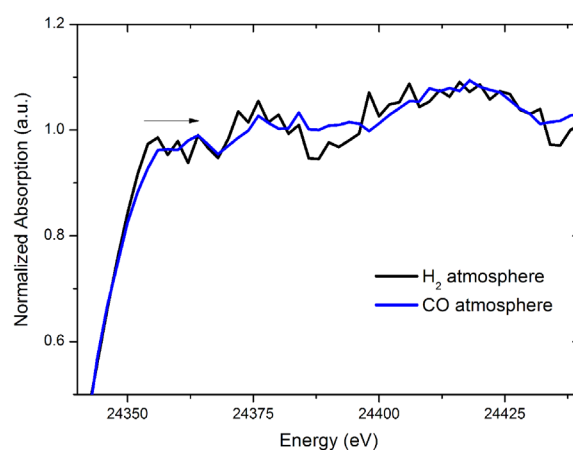


Figure 5. XANES close-up for Sample A-1 under H₂ and CO atmosphere. The slight shift towards higher energy of the XANES under CO can be attributed to PdC formation at ca. 24.69 keV.

The relatively high quantity of PdO (according to linear combination fitting) in the H₂ atmosphere could be explained by the fact that the nanoparticles are generally small (we calculate that 53% of the atoms in the nanoparticle are located at the surface) and the surface oxide layer (particularly at the metal: support interface) is difficult to completely remove particularly considering the comparatively low temperature at which the experiment is performed [22–24]. However, one should also be aware that some “unknown” error will be associated with using bulk reference samples to fit data from nanoparticles.

Figure 6 shows the various XANES spectra of sample B-1 under identical gas atmospheres to that of sample A-1. The first thing of empirical note is that the intensity of the “peaks” at 24.38 and 24.42 keV for the sample in a H₂ atmosphere are weaker in this sample although the feature at 24.37 keV is slightly greater; these observations

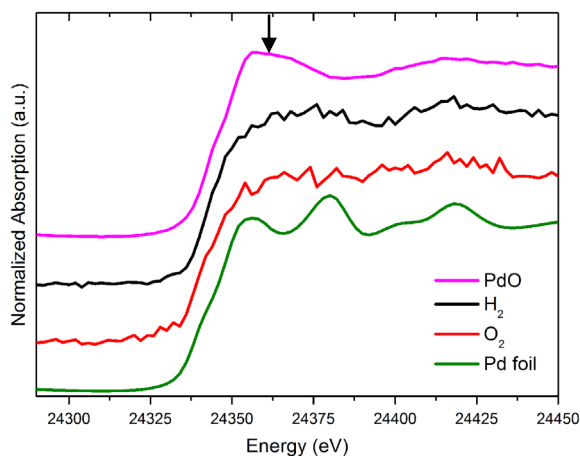


Figure 6. XANES spectra of sample B-1 under different atmospheres, including Pd foil and PdO standard; an arrow points out a Pd XANES feature at 24.37 keV.

suggest the nanoparticles to be both larger and more metallic, when compared to those seen in sample A-1. Interestingly, there is no change in the Pd K-edge XANES when switching to an O₂ atmosphere, suggesting that the residual polymer remaining on the nanoparticles after preparation limits the accessibility of the reactive gases (particularly O₂) to the Pd nanoparticles. Importantly we note that these data are recorded from only ~20 nanoparticles and over a time scale (minutes) that would be relevant for measuring nanoparticle response in a reactive gas atmosphere.

4. Conclusions and future outlook

In this study we successfully obtained uniform Pd nanoparticles using a reverse micelle synthesis method and demonstrated that it was possible to obtain spectroscopic information using a nanosized X-ray beam from as few as ~20 nanoparticles (we estimate) allowing us to analyse nanoparticle behaviour under various reactive gas atmospheres at fixed temperatures. The preliminary data presented in this manuscript is the first attempt to examine single nanoparticles, which could help remove statistical averaging effects that accompanies bulk XAS techniques. For example, we were able to follow partial reduction and re-oxidation reactions that small Pd nanoparticles in sample A-1 undergo. In one case, due to low signal/noise ratio, it is not possible to distinguish quantitatively, through linear combination fitting, the amount of palladium carbide species present. However, an observed energy shift allows for a qualitative interpretation of the spectra to demonstrate the presence of a PdC component [21]. This enables the identification of changes occurring due to the interaction of gases with the nanoparticles. We also demonstrate that whilst it is possible to create metal nanoparticle populations using

an advanced reverse micelle technique, the polymeric species on the surface must be removed adequately, or as demonstrated over sample B-1, nanoparticles can effectively be shielded from reactive gases.

Due to significant improvements in synchrotron brightness, focusing optics and detection it is now becoming much easier to obtain X-ray beams with dimensions in the nanometre regime and from which spectroscopic data (essentially XANES although it is anticipated that EXAFS data will be obtainable in the future) can be obtained. However, there are still challenges to be overcome before for example, the real effects of nanoparticle size can be determined in catalytic systems, particularly under operando conditions and this mainly concerns the data quality. This could be approached from two perspectives; the sample and the setup. The former would require that the number of nanoparticles/nanoparticle density would ideally need to be increased by tuning the synthesis method although there is a risk that this could compromise the uniformity of the size and one should also consider the impact that this would have on the space velocities needed for experiment. Alternatively, as newer fluorescence/photon counting detectors are developed, this compromise can be brought to lower thresholds and thus towards single nanoparticle analysis for applications such as particle size and shape effects in catalysis, or single nanoparticle growth mechanisms. From the standpoint of probing catalysis, low temperature reactions, such as CO oxidation or butadiene hydrogenation would be feasible in the current set up and will be carried out in the future [25]. However, for reactions such as Fischer-Tropsch synthesis, often carried out at temperatures upwards of 473 K, and pressures of 20 bar, the current set up would have to be adapted. The reactor might be replaced with Al for example, to withstand larger temperatures, but sourcing a way to pre-heat the gas without heat loss or affecting the surrounding beamline optics would be a challenge. Furthermore, SiN_x windows would likely have to be thickened to withstand such pressures (or an alternative compound used if the windows cannot withstand the pressure) – which will invariably lead to a decrease in signal to noise as the X-ray path length would increase. Another challenge would be investigating systems where the catalyst of choice is a 1st row transition metal. Whilst high Z elements have a large fluorescence yield, such as Pd – used here, lower Z elements such as 1st row transition metals will present even more of a challenge as the fluorescence yield is lower. However, these challenges are not insurmountable and it is clear that things are moving rapidly towards a better understanding of nanoparticle size/behaviour and their catalytic properties, and in particular using the setup in this study will enable the accurate determination of particle size effects on catalysis in the future.

Acknowledgements

EPSRC and ESRF are kindly acknowledged for financial support and access to beamline facilities.

Disclosure statement

No potential conflict of interest was reported by the authors.

Funding

This work was supported by Engineering and Physical Sciences Research Council [grant number EP/K007467/1].

ORCID

David James Martin  <http://orcid.org/0000-0002-3549-4202>
Andrew M. Beale  <http://orcid.org/0000-0002-0923-1433>

References

- [1] Gibson EK, Beale AM, Catlow CRA, et al. Restructuring of AuPd nanoparticles studied by a combined XAFS/DRIFTS approach. *Chem Mater*. 2015;27:3714–3720.
- [2] Cuenya BR. Metal nanoparticle catalysts beginning to shape-up *Acc Chem Res*. 2013;46:1682–1691.
- [3] Bond GC. The origins of particle size effects in heterogeneous catalysis. *Surf Sci*. 1985;156:966–981.
- [4] Reske R, Mistry H, Behafarid F, et al. Particle size effects in the catalytic electroreduction of CO₂ on Cu nanoparticles. *J Am Chem Soc*. 2014;136:6978–6986.
- [5] Nesselberger M, Ashton S, Meier JC, et al. The particle size effect on the oxygen reduction reaction activity of Pt catalysts: Influence of electrolyte and relation to single crystal models. *J Am Chem Soc*. 2011;133:17428–17433.
- [6] van den Berg R, Prieto G, Korpershoek G, et al. Structure sensitivity of Cu and Cu₂N catalysts relevant to industrial methanol synthesis. *Nat Commun*. 2016;7:20457–20465. DOI:10.1038/ncomms13057
- [7] Nolte P, Stierle A, Jin-Phillipp NY, et al. Shape changes of supported Rh nanoparticles during oxidation and reduction cycles. *Science*. 2008;321:1654–1658.
- [8] Rogers SM, Catlow CRA, Chan-Thaw CE, et al. Tailoring gold nanoparticle characteristics and the impact on aqueous-phase oxidation of glycerol. *ACS Catal*. 2015;5:4377–4384.
- [9] Spatz JP, Mössmer S, Hartmann C, et al. Ordered deposition of inorganic clusters from micellar block copolymer films. *Langmuir*. 2000;16:407–415.
- [10] Laforce B, Schmitz S, Vekemans B, et al. Nanoscopic x-ray fluorescence imaging of meteoritic particles and diamond inclusions. *Anal Chem*. 2014;86:12369–12374.
- [11] Martinez-Criado G, Villanova J, Tucoulou R, et al. ID16B: a hard x-ray nanoprobe beamline at the ESRF for nano-analysis. *J Synchrotron Radiat*. 2016;23:344–352.
- [12] Crozier PA, Hansen TW. In situ and operando transmission electron microscopy of catalytic materials. *MRS Bull*. 2015;40:38–45.
- [13] Sambur JB, Chen P. Approaches to single-nanoparticle catalysis. *Annu Rev Phys Chem*. 2014;65:395–422.
- [14] Mino L, Agostini G, Borfecchia E, et al. Low-dimensional systems investigated by x-ray absorption spectroscopy: a selection of 2D, 1D and 0D cases. *J Phys D Appl Phys J Phys D Appl Phys*. 2013;46:423001–423001.
- [15] Herbert JJ, Senecal P, Martin DJ, et al. x-ray spectroscopic and scattering methods applied to the characterisation of cobalt-based Fischer-Tropsch synthesis catalysts. *Catal Sci Technol*. 2016;6:5773–5791.
- [16] Spatz JP, Sheiko S, Möller M. Ion-stabilized block copolymer micelles: film formation and intermicellar interaction. *Macromolecules*. 1996;29:3220–3226.
- [17] Spatz JP, Mößmer S, Möller M. Mineralization of gold nanoparticles in a block copolymer microemulsion. *Chem – A Eur J*. 1996;2:1552–1555.
- [18] Ravel BNM, Newville M. Data analysis for x-ray absorption spectroscopy using ifeffit. *J Synchrotron Radiat*. 2005;12:537–541.
- [19] Sun Y, Frenkel AI, Isseroff R, et al. Characterization of palladium nanoparticles by using x-ray reflectivity, EXAFS, and electron microscopy. *Langmuir*. 2006;22:807–816.
- [20] Beale AM, Weckhuysen BM. EXAFS as a tool to interrogate the size and shape of mono and bimetallic catalyst nanoparticles. *Phys Chem Chem Phys*. 2010;12:5562–5574.
- [21] Bugaev AL, Guda AA, Lazzarini A, et al. In situ formation of hydrides and carbides in palladium catalyst: when XANES is better than EXAFS and XRD. *Catal Today*. 2015. DOI:10.1016/j.cattod.2016.02.065
- [22] Luch A. Molecular, Chapter 8 Nanomaterials: A Challenge for Toxicological Risk Assessment?, *Clinical and Environmental Toxicology: Volume 3: Environmental Toxicology*. Berlin (Germany): Springer Science & Business Media. 2012;101.
- [23] Lead JR, Smith E. Environmental and human health impacts of nanotechnology. Chichester (UK): Wiley Online Library; 2009. p. 151–179.
- [24] Otto K, Haack LP, deVries JE. Identification of two types of oxidized palladium on gamma-alumina by x-ray photoelectron spectroscopy. *Appl Catal B Environ*. 1992;1:1–12.
- [25] Peterson EJ, DeLaRiva AT, Lin S, et al. Low-temperature carbon monoxide oxidation catalysed by regenerable atomically dispersed palladium on alumina. *Nat Commun*. 2014;5:4885.